

# Modelling laser beam absorption for powder-based sintering

Albert Hendrik Nijkamp<sup>1,\*</sup>, Juan Esteban Alvarez<sup>1</sup>, Stefan Luding<sup>1</sup>, and Thomas Weinhart<sup>1</sup>

<sup>1</sup>Multi-Scale Mechanics, ET, TFE, University of Twente, Drienerlolaan 5, 7522 NB Enschede, The Netherlands

**Abstract.** Additive manufacturing techniques like selective laser sintering face challenges such as residual stresses and warping. Understanding laser-powder interaction is crucial to addressing these issues. This paper presents a computational model to simulate laser energy propagation and absorption in a particle bed during early sintering stages. A ray tracing model, developed in MATLAB®, simulates light propagation through 2D and 3D particle beds. The 2D model is used to identify several numerical parameters for the 3D model, which is applied to a particle doublet. Its results are then used for mechanical sintering simulations in MercuryDPM. These model predictions are compared to experimental data on the sintering of polystyrene particles. The model is extended to a full 3D particle bed used to derive equations which can efficiently estimate absorbed energy per particle based on material, geometric, and laser parameters. A semi-random walk is also introduced, simulating light propagation stochastically while significantly reducing computation time. This stochastic approach yields energy distributions in the particle bed comparable to ray tracing but is 1000 times faster. Lastly, equations are derived that replace the simulations, further reducing the computation time by a factor of 70, making them suitable for transient sintering simulations.

## 1 Introduction

One of the many methods in additive manufacturing is selective laser sintering (SLS). Here, a laser beam penetrates into a powder bed, causing the particles to sinter together. However, SLS has some known issues such as residual stresses inside the material and shrinkage or warping of the printed parts. These issues can be a result of a too-low chamber temperature, a too-high cooling rate after printing, or a non-uniform bed temperature [1]. Performing experiments and computational simulations of sintering particles can help to give a better understanding of the underlying phenomena causing these problems. A proper model of the laser energy absorption by the particles is necessary to produce models which are capable of realistically simulating the sintering of powder beds.

In previous studies, Hejmady et al. analysed the light absorption and sintering of polystyrene (PS) [2] and polyamide 12 (PA12) particles [3]. Two particles were sintered using a laser while changing several variables. The neck radius and temperature evolution were measured. These experimental results are used in this study to calibrate several variables necessary for the simulation of sintering particles in MercuryDPM [4]. Here, two different materials were simulated: PA12 and PS. While PA12 is a suitable crystalline material for SLS, PS is an amorphous polymer which does not have a clear melting temperature [1]. However, amorphous polymers such as PS in general come with a lower price compared to PA12 and are therefore still often used in AM [5]. Therefore, both materials have been used for the simulations.

This study introduces a laser absorption model which focuses on the particle scale. A laser beam is discretised

into a finite number of rays which propagate in the particle bed. Several simulation variables and their effect on the absorption are analysed in both 2D and 3D in section 2: Ray tracing absorption model. In section 3: Model simplification, two types of simplifications are proposed to replace the ray tracing simulations: a set of equations which are computationally friendly to execute, and the use of a semi-random walk. This way, the light absorption of the particles can be calculated quickly, and subsequently be used in the particle sintering simulations in MercuryDPM. For both simplifications, variable dependencies were incorporated which results in an absorption model where different bed and material properties can be used.

## 2 Ray tracing absorption model

The structure of polymer chains determines the opacity of a material, with opaque materials scattering more light, which is a difference between amorphous and crystalline polymers. The light path and absorption also depend on the light wavelength and particle shape [6]. For simplicity, this study assumes no internal scattering for both materials and perfectly spherical, monodisperse particles. This makes it possible to calculate the expected path for each ray interacting with a particle.

### 2.1 Ray tracing absorption model

To describe the energy absorption of a laser in powder beds, the incoming light beam is discretised and modelled as a finite number of rays, each having its own path while propagating into the bed. This model was presented by

\* Corresponding author: [a.h.nijkamp@alumnus.utwente.nl](mailto:a.h.nijkamp@alumnus.utwente.nl)

Osmanlic et al. [7] and is used in this study. In his model, each ray is traced through particles where it is partly absorbed, until it is completely absorbed or has left the bed. During this tracing, the rays undergo reflection and transmission/refraction when interacting with the particles.

Each ray has an energy  $I$  [-] while every particle has an energy absorption  $E$  [-], both expressed as a portion of the total laser energy. If a ray propagates inside the material for a distance  $z$ , then the particle will absorb the laser energy, causing the energy of the ray to decrease exponentially from  $I_0$  to  $I_l$  according to the Beer-Lambert law:

$$I_l = I_0 \exp(-\mu z) \quad (1)$$

with  $\mu$  the attenuation coefficient of the material. If a ray propagates inside air, the light energy remains constant as there is no interaction between atmospheric air and visible light, especially if the light contains high-energy photons [8]. This is similar for gases such as nitrogen and argon, which are often used in SLS, as they exhibit negligible interaction with CO<sub>2</sub> laser light [9]. Once a ray interacts with a particle and splits into two new rays, its energy is divided among the transmitted and reflected ray using the reflected energy portion factor  $R$ :

$$R = \frac{1}{2} \left( \left( \frac{n_A \cos \alpha - n_B \cos \beta}{n_A \cos \alpha + n_B \cos \beta} \right)^2 + \left( \frac{n_B \cos \alpha - n_A \cos \beta}{n_B \cos \alpha + n_A \cos \beta} \right)^2 \right) \quad (2)$$

with  $n_A$  and  $n_B$  the refraction index of air and the particle,  $\alpha$  the incoming angle and  $\beta = \sin^{-1}((n_A/n_B) \sin(\alpha))$  the transmitted angle. This gives the reflected ray an energy of  $IR$  and the transmitted ray an energy of  $I(1 - R)$  where  $I$  is the energy before the ray splits.

Firstly, the model is analysed on 2D cases to establish some numerical variables, after which 3D cases are analysed. All ray tracing simulations are steady-state and done in MATLAB®. Using the results of Hejmady et al. [2], attenuation coefficients of  $\mu = 27400 \text{ m}^{-1}$  for PS and  $\mu = 33500 \text{ m}^{-1}$  for PA12 are achieved, and assumed to be independent of temperature. Furthermore,  $n_B = 1.5997$  for PS [10] and  $n_B = 1.525$  for PA12 [11] are used, and  $n_A = 1$ .

## 2.2 2D simulations

Several 2D simulations were made that simulate light rays propagating through a particle bed, represented by circles with a diameter  $D$ . The light rays start equidistantly on a line above the particles, and are updated after a spatial step size  $\Delta l$ , where the ray energy is updated using Eq. (1) and the ray direction  $\mathbf{k}$  is updated based on a change in medium. Three numerical variables were determined:

- The initial number of rays  $N_{ray}$ , together representing the laser beam with an almost infinite number of rays.
- The spatial step size  $\Delta l$ , which can be seen as the discretisation of the ray paths.
- The energy dissipation threshold  $I_{min}$ , which determines when the rays stop propagating, defined as a percentage of the average starting energy of the rays ( $1/N_{ray}$ ).

After every spatial step, the simulation checks whether a ray is fully dissipated or has left the bed, and is finished when this is the case for all rays. From the simulations,  $I_{min} = 0.01/N_{ray}$  showed a good balance between accuracy and simulation time. For  $\Delta l$ , it was found that a too-high value could result in missed interactions with a particle. A

value of  $\Delta l < 0.1D$  showed less than 3% variation in absorbed energy, which was similar for the 3D simulations, and was therefore used in the following simulations. The variable  $N_{ray}$  proved to be case-specific. It depended on the position of the particles and the required level of precision. Several values were tested to find a good balance between accuracy and calculation time, but for most 3D simulations,  $10^4$  rays were used.

## 2.3 3D simulations

For the 3D simulations, a set of rays with starting points within a circle or ellipse positioned above the particle bed is used to represent a laser beam. The particle bed, consisting of monodisperse spheres, is generated using MercuryDPM [4]. Yaagoubi et al. [12] showed that the laser energy distribution for CO<sub>2</sub> lasers, common in SLS, can be approximated by a Gaussian curve and that twice the standard deviation can be used for the laser radius  $r_{laser}$ . By rotating and integrating the curve, the total energy is achieved and set to 1. The starting positions of the rays are randomly distributed over the beam, therefore each ray occupies an average area of  $\pi r_{laser}^2 / N_{ray}$ . The Gaussian curve divided by this area determines the energy for each ray:

$$I_0(d, r_{laser}, N_{ray}) = \frac{C_0}{N_{ray}} \exp\left(\frac{-2d^2}{r_{laser}^2}\right) \quad (3)$$

with  $C_0 = 2/(1 - \exp(-2)) \approx 2.3$ ,  $I_0$  the laser energy and  $d$  the distance of the ray to the laser centre. Initially, each ray is given a coordinate, a direction  $\mathbf{k}$ , and an energy according to Eq. (3). Once the simulation is finished, the absorbed energy  $E$  for each particle is determined, which can be used to calculate its temperature change  $\Delta T$  per time step  $\Delta t$ . Hejmady et al. [2] showed that due to a small Biot number ( $Bi \ll 0.1$ ), a homogeneous particle temperature can be assumed:

$$\Delta T = \frac{P_{in} E \Delta t}{m c_p} \quad (4)$$

with  $P_{in}$  the laser power,  $m$  the particle's mass and  $c_p$  the specific heat capacity. This  $\Delta T$  was implemented by Alvarez et al. [13] in MercuryDPM to describe the particles' temperature evolution during transient sintering simulations. His model also simulates the thermal diffusion in the bed and the viscous flow of the particles using the absorption model presented here, which focuses on the propagation of the laser beam and the heating of the particles.

## 3 Model simplification

To decrease the simulation time, two types of simplifications will be introduced: a set of equations for a particle doublet and a powder bed, and the use of a random walk.

### 3.1 Replacement equations for a particle doublet

To calibrate some variables for sintering simulations in MercuryDPM, experiments by Hejmady et al. [2] were used for comparison. Here, a PS particle doublet was created by shining a laser onto two spherical particles with equal diameter  $D$  on a reflective floor while measuring their overlap. The relative overlap  $\delta_n$  is the overlap divided by

the diameter. The respective simulation in MercuryDPM uses a set of replacement equations to calculate the energy absorption  $E$  for each particle, which are based on the ray tracing simulations. Several values for  $\delta_n$  and  $D$  were simulated, corresponding to the values used in the experiment.  $E$  is plotted against  $\delta_n$  in Fig. 1:

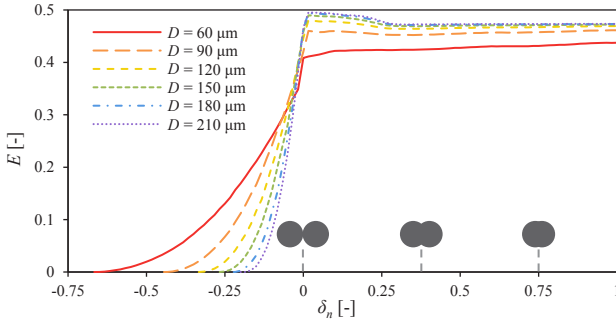


**Fig. 1.** Energy absorption  $E$  per particle for particle doublet with varying diameter  $D$  and relative overlap  $\delta_n$  for  $r_{laser} = 20 \mu\text{m}$ .

Each line shows the energy absorption at a certain  $\delta_n$  for a given  $D$ . Fitting curves for each diameter were found in the form of a 6<sup>th</sup>-order polynomial, with  $\delta_n$  as the input and  $E$  as the output. These equations were used in MercuryDPM and the results were compared to Hejmady's experiments [14], which is not shown in this study.

### 3.2 Replacement equations for a powder bed

Equations can also be derived for a whole bed of particles. The variables which are expected to affect the energy absorption are the particle diameter  $D$ , density  $\rho$ , refraction index ratio  $x = n_A/n_B$ , attenuation coefficient  $\mu$  and position relative to the laser; the bed volume fraction  $\phi$ ; and the laser power  $P_{in}$  and radius  $r_{laser}$ .

Firstly, the energy absorption of the particles in the top layer is derived.  $E_p$  is the portion of energy a particle absorbs out of what it receives and is calculated by integrating the energy absorption at every position on the particle over the top surface area of this particle:

$$E_p(x, \mu, D) = \int_0^1 \frac{1}{\frac{1}{1-R} - \frac{1}{1 - \exp(\mu D \sqrt{1-x^2 r^2})}} dr \quad (5)$$

However, this integral was found to be unsolvable. The trapezoidal integral approximation was used as an estimation. If the argument of the integral is defined as  $f(r)$ , then:

$$E_p(x, \mu, D) = \int_0^1 f(r) dr \approx \frac{1}{n} \sum_{i=1}^{n-1} f\left(\frac{i}{n}\right) \quad (6)$$

where a larger step-number  $n$  has a larger accuracy. A value of  $n = 500$  shows a maximum deviation of less than 0.1% of the true value. As an example,  $n_A = 1$ ,  $n_B = 1.5997$ ,  $\mu = 27400 \text{ m}^{-1}$  and  $D = 60 \mu\text{m}$  give  $E_p \approx 0.705$ , thus 70.5% of the light which hits a particle is absorbed.

$E_{in}$  is the portion of energy a particle receives out of the total laser energy, and can be calculated by integrating the laser energy over the top surface area of a particle:

$$E_{in}(d, D, r_{laser}) = \int_A^B \frac{2d_s C_0}{\pi r_{laser}^2} e^{-\frac{2d_s^2}{r_{laser}^2} \cdot \text{real}} \left( \cos^{-1} \left( \frac{d_s^2 + d^2 - (D/2)^2}{2d_s d} \right) \right) dd_s \quad (7)$$

with  $A = \max(d - D/2, 0)$  and  $B = \min(d + D/2, r_{laser})$ , accounting for particles overlapping with the laser centre or

edge.  $d_s$  is the distance of any point within the particle to the laser centre. Again, this integral was found to be unsolvable and the trapezoidal integral approximation was used. If the argument of the integral is defined as  $f(d_s)$ , then:

$$E_{in}(d, D, r_{laser}) = \int_A^B f(d_s) dd_s \approx \frac{B-A}{n} \sum_{i=1}^{n-1} f\left(A\left(1 - \frac{i}{n}\right) + B\frac{i}{n}\right) \quad (8)$$

Here,  $n = 1000$  steps showed a maximum deviation of less than 0.1%. For  $d = 0 \mu\text{m}$ ,  $D = 60 \mu\text{m}$  and  $r_{laser} = 200 \mu\text{m}$  give  $E_{in} \approx 0.0508$ , thus a top-layer particle located at the centre of the laser receives 5.08% of the total laser energy.

The two values  $E_p$  and  $E_{in}$  can be multiplied to achieve the total energy absorption of a top-layer particle,  $E_{abs} = E_p E_{in}$ . The example numbers show  $E_{abs} = 0.0358$ , thus this particle absorbs 3.58% of the laser energy.

Some rays reflecting away from top layer particles hit neighbouring particles and do not leave the bed. A factor of  $K_{cor} = 1.09937$  was found to correct this, and appeared to be independent of  $\phi$ ,  $x$ ,  $\mu$  or  $D$ . This gave a coefficient of determination of  $R^2 = 0.99646$  for the top layer particles compared to the ray tracing simulation.

To calculate the absorption for the rest of the bed, the absorption in the top layer is multiplied by a depth factor  $K_{depth}$ . This factor was found by choosing a function shape based on the ray tracing simulation results, and iteratively optimising its parameters until the highest  $R^2$  was found.

$$K_{depth} = \exp((F + G(\mu D)^H)(\mu z)^I + J(\mu z)^K \cdot (\phi - L)^M) \quad (9)$$

with eight factors:  $[F G H I J K L M] = [-0.036 -0.45 -0.48 1.4 -3.8 0.3 0.574 0.8]$ . This equation includes the effect of the attenuation coefficient, particle size and volume fraction on the system, and the particle depth parallel to the laser  $z$ :

$$z = (i - 1)D\sqrt{6}/3 \cos \theta \quad (10)$$

with  $\theta$  the laser angle and  $i$  the theoretical layer number of a particle, as monodisperse spheres naturally group into layers with a height of  $D\sqrt{6}/3$ . This ensures that the tops of the particles in the top layer have a depth of  $z = 0$ . Since laser angles in SLS are in general up to  $20^\circ$  [15], several laser angles were tested using the ray tracing simulations, but no significant change in absorbed energy was found.

Lastly, Eq. (8) uses  $d$ , the perpendicular distance to the laser centre, which can be calculated with:

$$d = \frac{|(\bar{c} - \bar{p}_p) \times \mathbf{k}_0|}{|\mathbf{k}_0|} \quad (11)$$

with  $\bar{c}$  the coordinates of the laser centre along the laser beam,  $\bar{p}_p$  the coordinates of the particle centre and  $\mathbf{k}_0$  the initial laser direction. When testing different refraction index ratios, no difference in absorption was found. The absorption for any particle can now be calculated with:

$$E = E_{abs} K_{cor} K_{depth} \quad (12)$$

The final  $R^2$  value, averaged out over volume fractions ranging from 0.575 to 0.7 (corresponding to non-overlapping particle beds), resulted into  $R^2 = 0.9619$ .

### 3.3 Semi-random walk approximation

The semi-random walk is similar to the ray tracing simulations, but uses rays that stochastically change direction

inside a volume with virtual particles, using rules based on the ray tracing simulations. Rays again start randomly distributed in a circle with a downward direction and a total energy of 1. After a certain random distance  $l_{air}$  the ray changes from medium A to B at a random point on a generated sphere. Then, reflection and refraction occur as normal. Based on the point of interaction on the sphere, the ray splits up into a reflected and transmitted ray with new directions and energies, at both the entry and exit point. The value for  $l_{air}$  depends on the volume fraction  $\varphi$  and is random with a certain probability distribution, which is acquired using the ray tracing simulations. Here, the ray distances between particles were analysed and a distribution was found using `histfit()` in MATLAB®. Then, a fitting curve was found for several values of  $\varphi$ . Using this equation for the distribution,  $l_{air}$  can be determined during the random walk. The distance to the first particle interaction in the top layer,  $l_{start}$ , follows a different distribution. For this, a similar approach was used.

The results of the random walk showed similar energy absorptions compared to the ray tracing simulations. However, since virtual particles are used, the absorption can only be calculated by adding particles together within a region to say something about the absorption within that region. The random walk does not define the absorption a particle would have at a specific point in the bed.

## 4 Conclusions

A detailed understanding of laser-powder interactions is necessary to improve the selective laser sintering process and to address challenges such as residual stresses, warping, and non-uniform sintering. In this study, a ray tracing model was developed to simulate laser energy absorption in 2D and 3D particle beds, capturing the complex interaction between laser light and powder particles.

To reduce the high computational cost of full ray tracing, two simplifications were introduced: (1) replacement equations and (2) a semi-random walk approximation. As shown in Table 1, the replacement equations, when calibrated against the ray tracing results, reduce the computation time by a factor of 70000 while retaining a high accuracy ( $R^2 \approx 0.96$ ), making them well-suited for use in transient sintering simulations like MercuryDPM. The semi-random walk model also captures the overall energy distribution trends and provides a  $\sim 1000\times$  speed-up, but lacks the spatial resolution required for particle-specific predictions.

**Table 1.** Calculation times for a  $1\times 1\times 0.5$  mm bed with 2653 particles where  $D = 60 \mu\text{m}$ ,  $\varphi = 0.6$ ,  $\mu = 27400 \text{ m}^{-1}$  and  $x = 1/1.5997$ . For methods 1 and 2,  $r_{laser} = 200 \mu\text{m}$ , and for methods 1 and 3,  $N_{ray} = 10000$ .

Calc. method	1. Ray tracing simulation	2. Replacement equations	3. Semi-random walk
Calc. time	$\pm 5000$ s	$\pm 0.07$ s	$\pm 5$ s

The current model applies to monodisperse, spherical particles with bed volume fractions between 0.575 and 0.7. While the ray tracing simulations account for overlapping particles, the replacement equations do not, which constrains their applicability in highly agglomerated or dynamically evolving beds. Addressing this limitation, extending the model to polydisperse, irregularly shaped particles, and validating the equations with experimental data focused

on light propagation and absorption in powder beds are promising directions for future work.

## References

1. M.B. Sagar, K. Elangovan, Consolidation & factors influencing sintering process in polymer powder based additive manufacturing. in IOP Conference Series: Materials Science and Engineering **225**, 012075 (2017)
2. P. Hejmady, L.C.A. van Breemen, P.D. Anderson, R. Cardinaels, Laser sintering of polymer particle pairs studied by in situ visualization. *Soft Matter* **15**, 1373–1387 (2019)
3. P. Hejmady, L.C.A. van Breemen, D. Hermida-Merino, P.D. Anderson, R. Cardinaels, Laser sintering of PA12 particles studied by in-situ optical, thermal and X-ray characterization. *Addit. Manuf.* **52**, 102624 (2022)
4. T. Weinhart et al., Fast, flexible particle simulations — An introduction to MercuryDPM. *Comput. Phys. Commun.* **249**, 107129 (2020)
5. R. Brighenti, M.P. Cosma, L. Marsavina, A. Spagnoli, M. Terzano, Laser-based additively manufactured polymers: a review on processes and mechanical models. *J. Mater. Sci.* **56**, 961–998 (2021)
6. X. Liu, Numerical modeling and simulation of selective laser sintering in polymer powder bed, Ph.D. thesis, University of Lyon, France (2017)
7. F. Osmanlic et al., Modeling of laser beam absorption in a polymer powder bed. *Polymers* **10**, 784 (2018)
8. A.A. Kokhanovsky, *Light Scattering Reviews 10: Light Scattering and Radiative Transfer* (Springer, Berlin, 2016)
9. J. Greses, P.A. Hilton, C.Y. Barlow, W.M. Steen, Laser-Vapour Interaction in High-Power cw CO2 Laser Welding, in 22nd International Congress on Applications of Lasers & Electro Optics (2003)
10. N. Sultanova, S. Kasarova, I. Nikolov, Dispersion properties of optical polymers, in *Acta Physica Polonica A* **116**, 585–587 (2009)
11. Polymerdatabase, Nylon 12, available at: <http://polymerdatabase.com/polymers/nylon12.html> (Accessed: 12th May 2022)
12. H. Yaagoubi, H. Abouchadi, M. Taha Janan, Simulation of the Heat Laser of the Selective Laser Sintering Process of the Polyamide12. *E3S Web Conference* **297**, 01050 (2021)
13. J.E. Alvarez et al., Neck growth kinetics during polymer sintering for powder-based processes, in *EPJ Web Conference* **249**, 05001 (2021)
14. J.E. Alvarez, A.H. Nijkamp, H. Cheng, S. Luding, T. Weinhart, Contact rheological DEM model for viscoelastic powders during laser sintering. *Granul. Matter* **26**, 28 (2024)
15. C. Bibas, Traditional SLS/SLM 3D printing errors, available at: <https://tecnica.com/traditional-sls-slm-3d-printing-errors/> (Accessed: 19th October 2022)